Supporting Information

Highly efficient thermoelectric converters based on metalloporphyrin nanotubes

Qusiy H. Al-Galiby[1*], Laith A. Algharagholy[2], Hatef Sadeghi[3], Víctor M. García-Suárez[4*]

[1]Department of Physics, College of education, University of Al-Qadisiyah, Al Diwaniyah 58002, Iraq.
[2]Department of Physics, College of Science, University of Sumer, Al-Rifaee, 64005, Thi-Qar, Iraq.
[3]Device Modelling Group, School of Engineering, University of Warwick, Coventry CV47AL, UK.
[4]Departamento de Física, Universidad de Oviedo & CINN, Oviedo, 33007, Spain.
[*]Corresponding author: qusiy.algaliby@qu.edu.iq, vm.garcia@cinn.es

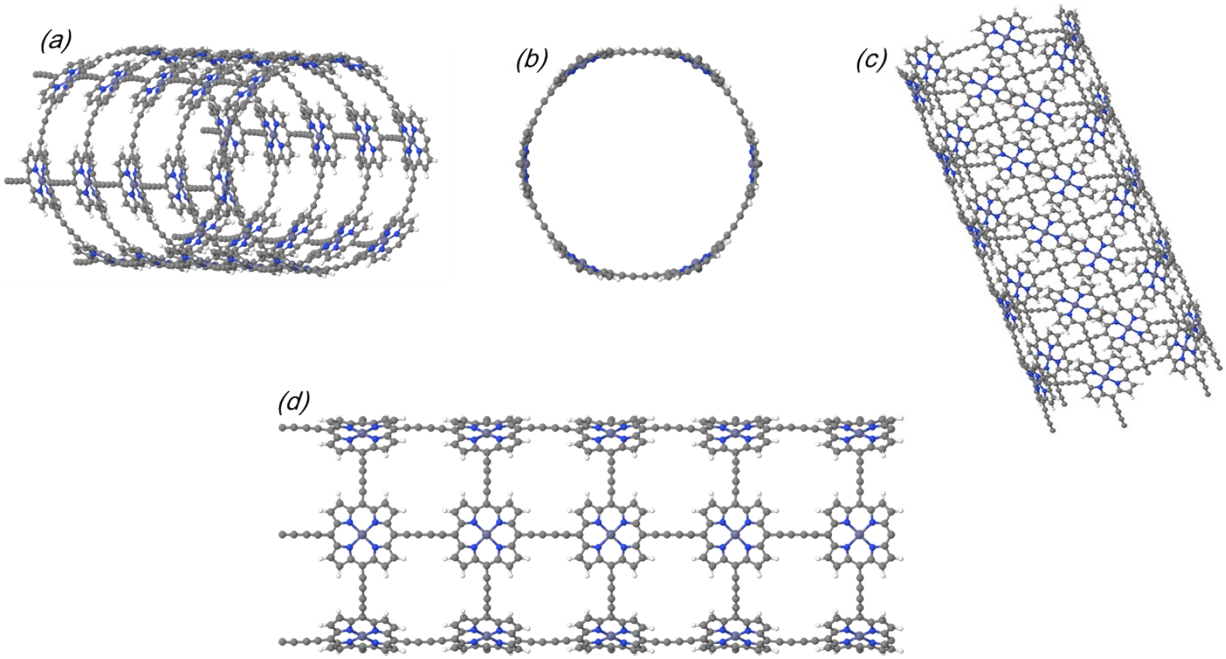

Figure S1. Different views of the calculated geometry of the metallo-porphyrin nanotube.

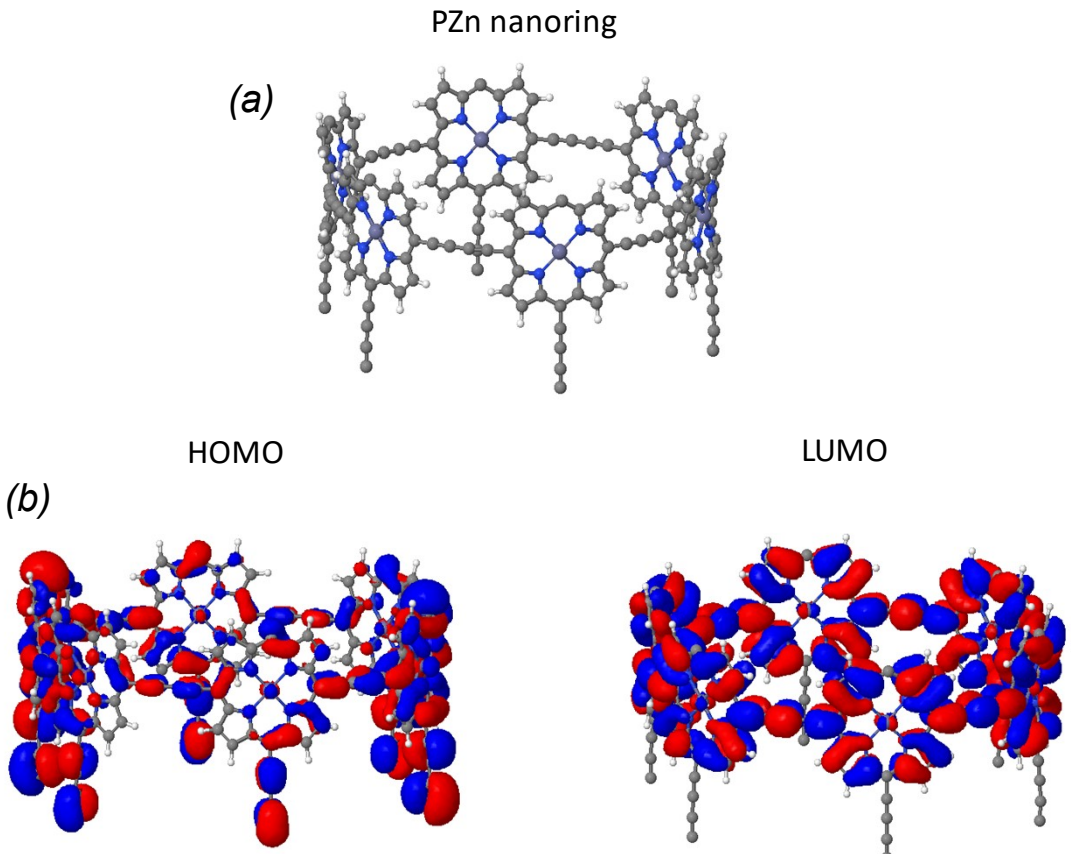

Figure S2. *(a)* Optimised geometry of the PZn nanoring (unit-cell). *(b)* Frontier molecular orbitals (FMOs) calculated with DFT-PBE. Red corresponds to positive and blue to negative regions of the wave functions.

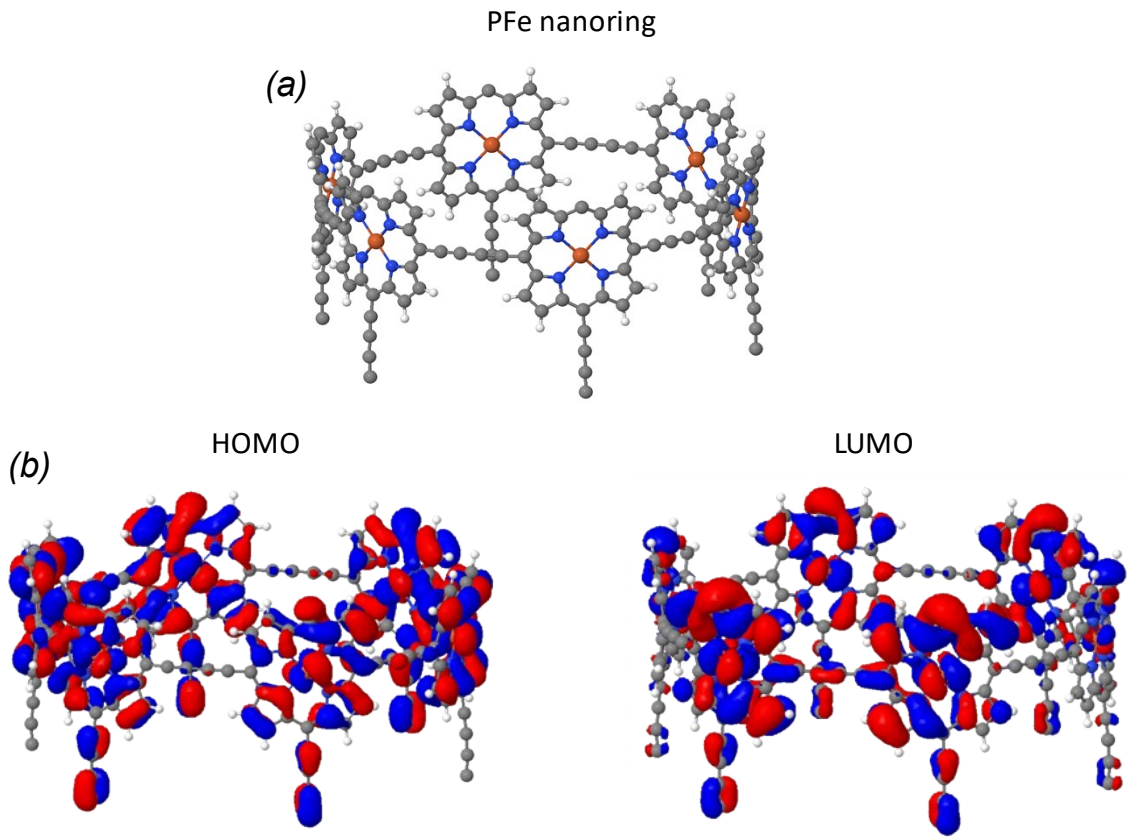

Figure S3. *(a)* Optimised geometry of the PFe(II) nanoring (unit-cell). *(b)* Frontier molecular orbitals (FMOs) calculated with DFT-PBE. Red corresponds to positive and blue to negative regions of the wave functions.

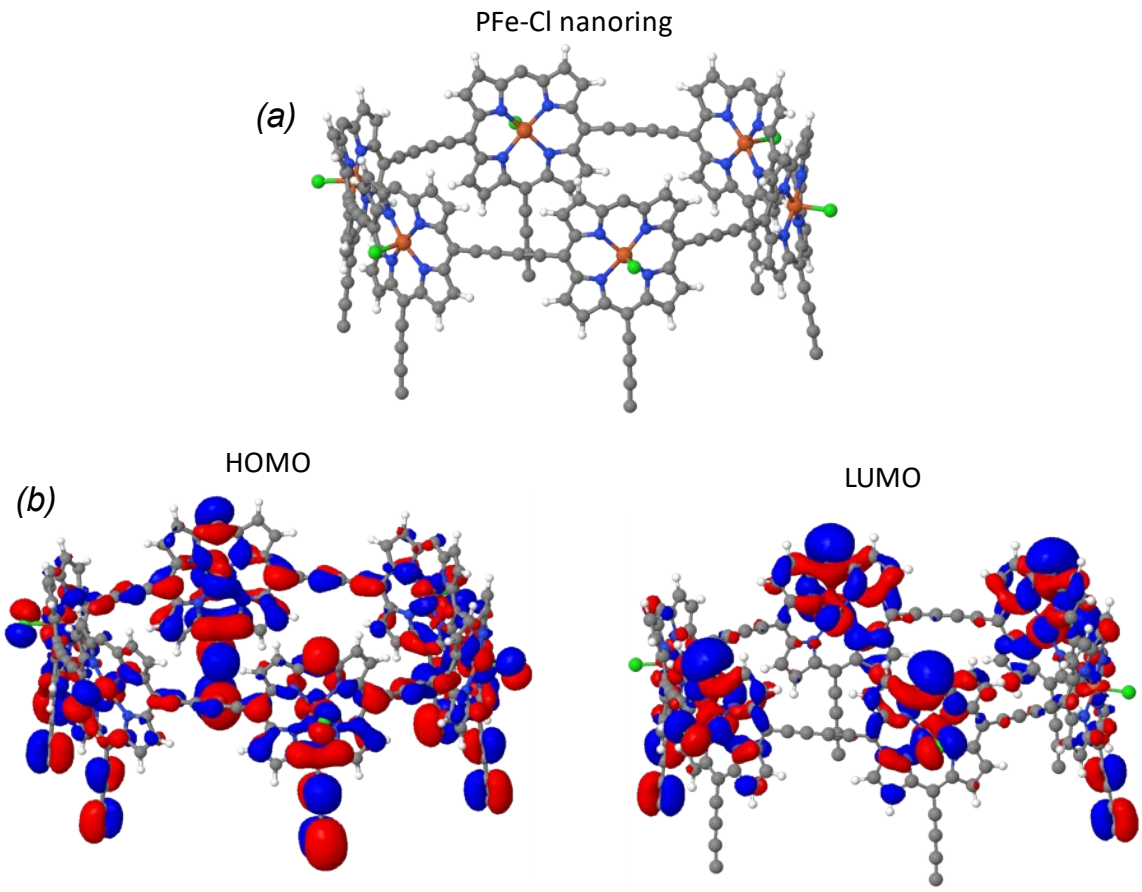

Figure S4. *(a)* Optimised geometry of the PFe(III)-Cl nanoring (unit-cell). *(b)* Frontier molecular orbitals (FMOs) calculated with DFT-PBE. Red corresponds to positive and blue to negative regions of the wave functions.

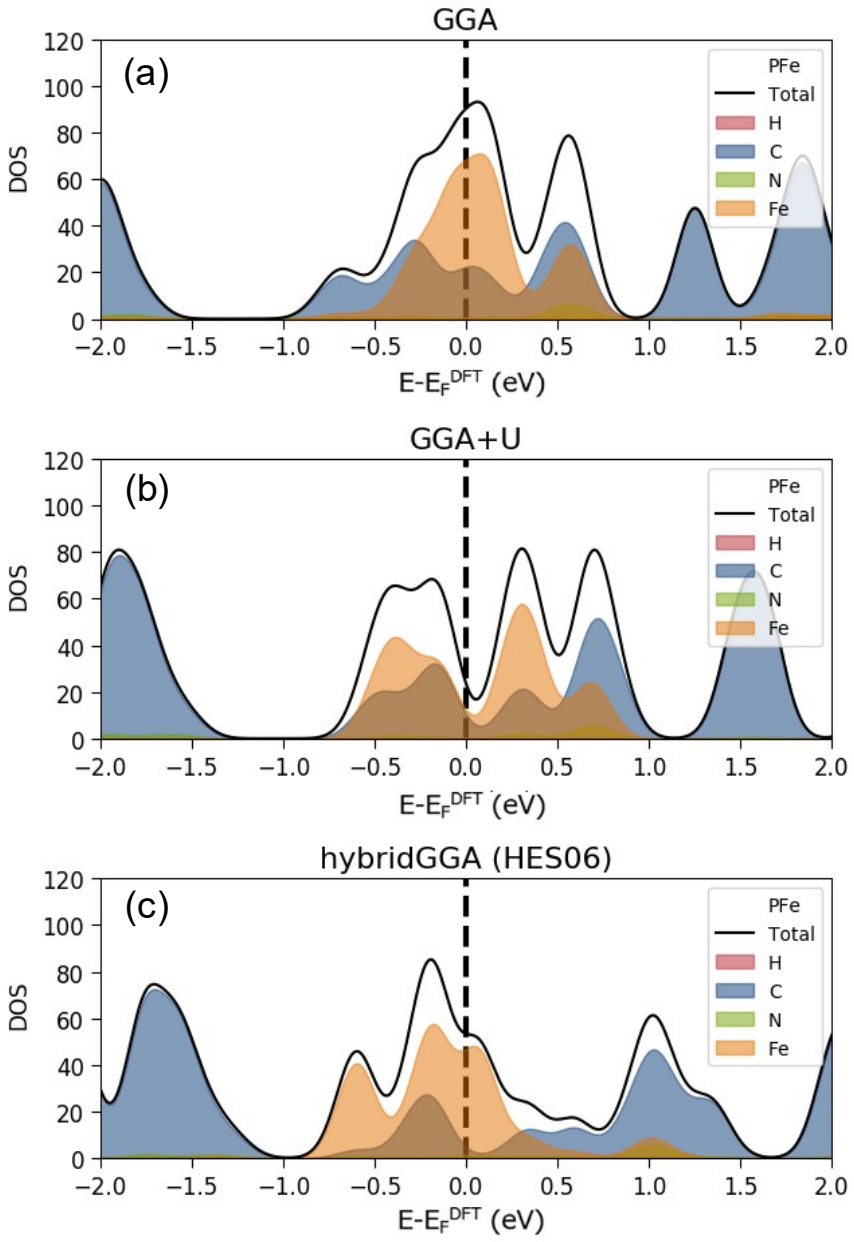

Figure S5. shows the DFT-calculation of density of states (DOS) for the PFe nanotube by using (a) GGA-PBE functional, (b) GGA+U and (c) hybrid functional GGA-HSE06.

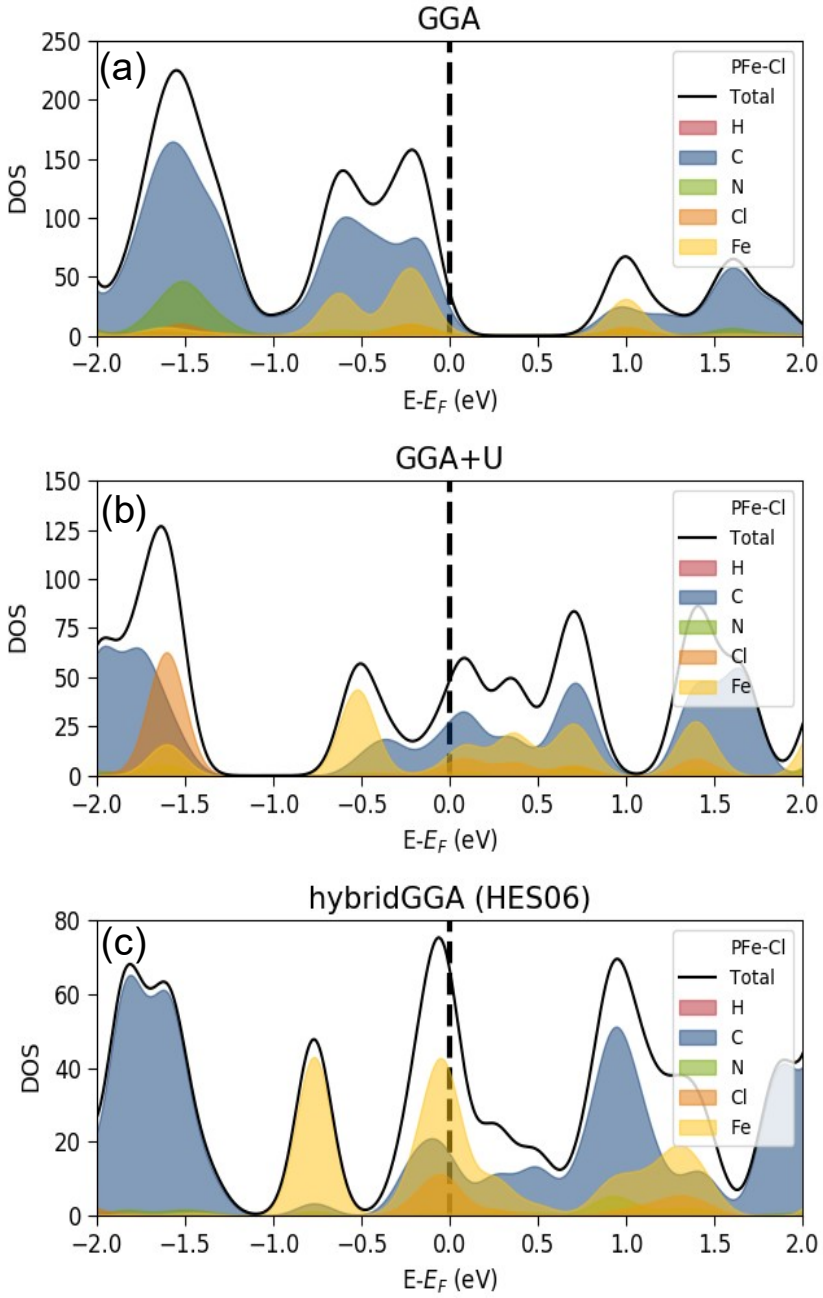

Figure S6. shows the DFT-calculation of density of states (DOS) for the PFe-Cl nanotube by using (a) GGA-PBE functional, (b) GGA+U and (c) hybrid functional GGA-HSE06.

Thermoelectric properties of metallo-porphyrin nanotubes

The non-normalized probability distribution $P(E)$ is defined by [1-3]

$$P(E) = -T(E)\frac{\partial f(E)}{\partial E}\ , \qquad (S1)$$

where $f(E)$ is the Fermi distribution function. The moments of $P(E)$ are

$$L_n = \int dE\ P(E)\left(E - E_F\right)^n. \qquad (S2)$$

The electrical conductance, G is given by the Landauer formula

$$G = \frac{2e^2}{h}L_0\ , \qquad (S3)$$

where h is Planck's constant. The normalised distribution $\rho(x)$ is defined by $\rho(x)=P(x)/L_0$. In terms of the moments L_n,

$$< x > \ = \frac{L_1}{L_0}, \quad \sigma^2 = \frac{L_2}{L_0} - \frac{L_1^2}{L_0^2}.$$

The thermopower (also known as the Seebeck coefficient S) is

$$S = -\frac{\Delta V}{\Delta T} = \frac{1}{eT}\frac{L_1}{L_0}. \qquad (S4)$$

The electronic contribution to the thermal conductance (k_e) is given by

$$k_e = \frac{21}{hT}L_0\ \left(\frac{L_2}{L_0} - \frac{L_1^2}{L_0^2}\right). \qquad (S5)$$

The electronic contribution to figure of merit (ZT_e) is

$$ZT_e = \left(\frac{S^2 G}{k_e}\right)T \qquad (S6)$$

For E close to E_F, if $T(E)$ varies only slowly with E on the scale of k_B then these formulae take the form

$$G(T) \approx \left(\frac{2e^2}{h}\right) T(E_F)\,, \qquad (S7)$$

$$S(T) \approx -\alpha e\, T \left(\frac{d\ln T(E)}{dE}\right)_{E = E_F} \qquad (S8)$$

$$k_e \approx L_0\, TG \qquad (S9)$$

where $\alpha = \left(\frac{k_B}{e}\right)^2 \frac{\pi^2}{3}$ is the Lorentz number. Equation (S8) shows that S is enhanced by increasing the slope of ln $T(E)$ near $E = E_F$. Hence, it is of interest to explore whether it is possible to move step-like feature in $T(E)$ close to E_F. In particular, in the present study, we will use one-dimensional organic nanostructures that can give rise to step-like feature in $T(E)$, located asymmetrically relative to E_F.

Strategies for increasing thermoelectric performance

To understand how transport resonances and quantum interference lead to high thermoelectric performance, we note that in the linear-response regime, the electric current I and heat current $\dot{Q}$ passing through a device is related to the voltage difference ΔV and temperature difference ΔT by [63]

$$\begin{pmatrix} I \\ \dot{Q} \end{pmatrix} = \frac{2}{h} \begin{pmatrix} e^2 L_0 & \frac{e}{T} L_1 \\ e L_1 & \frac{1}{T} L_2 \end{pmatrix} \begin{pmatrix} \Delta V \\ \Delta T \end{pmatrix} \qquad (S10)$$

where T is the reference temperature and

$$L_n = \int_{-\infty}^{\infty} (E - E_F)^n T(E) \left(-\frac{\partial f(E,T)}{\partial E}\right) dE \qquad (S11)$$

In this expression e=-|e| is the electronic charge, $T(E)$ is the transmission coefficient for electrons of energy E, passing through the molecule from one electrode to the other and $f(E,T)$ is Fermi distribution defined as $f(E,T) = [e^{(E - E_F)/k_B T} + 1]^{-1}$ where k_B is Boltzmann's constant.

In this expression e=-|e| is the electronic charge, $T(E)$ is the transmission coefficient for electrons of energy E, passing through the molecule from one electrode to the other and $f(E,T)$ is Fermi distribution defined as $f(E,T) = [e^{(E - E_F)/k_BT} + 1]^{-1}$ where k_B is Boltzmann's constant.

When $\Delta T = 0$, equation (S10) yields for the electrical conductance $G = (\frac{I}{\Delta V})_{\Delta T = 0}$,

$$G = \frac{2e^2}{h} L_0 \qquad (S12)$$

Similarly when $I = 0$, equation (S10) yields for the Seebeck coefficient $S = -(\frac{\Delta V}{\Delta T})_{I = 0}$,

$$S = \frac{-1 L_1}{|e| T L_0} \qquad (S13)$$

Equation (S10) can be rewritten in terms of the electrical conductance *(G)*, thermopower *(S)*, Peltier coefficient (∏), and the electronic contribution to the thermal conductance (κ_e):

$$\begin{pmatrix} \Delta V \\ \dot{Q} \end{pmatrix} = \begin{pmatrix} 1/G & S \\ \prod & \kappa_e \end{pmatrix} \begin{pmatrix} I \\ \Delta T \end{pmatrix} \qquad (S14)$$

where

$$\Pi = \frac{-1 L_1}{|e| L_0} \qquad (S15)$$

$$\kappa_e = \frac{2}{hT} \left(L_2 - \frac{(L_1)^2}{L_0} \right) \qquad (S16)$$

From the above expressions, the electronic thermoelectric figure $ZT_e = S^2GT/\kappa_e$ is given by

$$ZT_e = \frac{(L_1)^2}{L_0 L_2 - (L_1)^2} \qquad (S17)$$

Based on the above expressions, we now examine three strategies for increasing thermoelectric performance.

<u>Strategy 1: Utilising a steep slope in *T(E)*.</u>

For E close to E_F, if $T(E)$ varies approximately linearly with E on the scale of k_BT then $L_0 \approx T(E_F)$, $L_1 \approx (eT)^2\alpha\left(\frac{dT(E)}{dE}\right)_{E=E_F}$ and $L_2 \approx (eT)^2\alpha T(E_F)$, where α is the Lorenz number given by $\alpha = (\frac{1}{eT})^2 \int_{-\infty}^{\infty}(E-E_F)^2\left(-\frac{\partial f(E,T)}{\partial E}\right)dE = \left(\frac{k_B}{e}\right)^2\frac{\pi^2}{3}$ = 2.44.10^{-8} WΩK^{-2}. Hence in this limit, these formulae take the form [63]:

$$G \approx \left(\frac{2e^2}{h}\right)T(E_F), \qquad (S18)$$

$$S \approx -\alpha|e|T\left(\frac{d\,lnT(E)}{dE}\right)_{E=E_F}, \qquad (S19)$$

$$\kappa_e \approx \alpha TG. \qquad (S20)$$

Equation (S19) demonstrates that S is enhanced by increasing the slope of ln $T(E)$ and hence quantum-interference-induced resonances or other features in $T(E)$ with steep slopes close to E_F are desirable. To estimate what constitutes a "steep slope", we note that the Wiedemann-Franz Law, (Equation S20) yields

$$ZT_e = \frac{S^2}{\alpha} \qquad (S21)$$

Therefore in the low-temperature limit, if $ZT_e > 1$, then we require $S^2 > \alpha$, ie. $S > 150$ μV/K

<u>Strategy 2: Utilizing resonances in *T(E)*.</u>

Insight into alternative strategies for maximising ZT_e can be obtained by taking a 'statistical' view of Equations (S12, S13, S16 and S17), which demonstrates why the denominator of Equation (S17) must be positive from a mathematical viewpoint. If the Fermi energy of the reservoirs is E_F, then it is convenient to introduce the non-normalised distribution $P(E) = -T(E)\frac{\partial f(E)}{\partial E}$ and the corresponding normalized distribution $(E) = \frac{P(E)}{L_0}$. Then the mean of $(E-E_F)$ is $< E-E_F > = \int dE\,\rho(E)(E-E_F)$ and the variance is $\sigma^2 = < (E-E_F)^2 > - < E-E_F >^2$. This yields for Equation (S13)

$$S = \frac{-1}{|e|T} < E-E_F >, \qquad (S22)$$

Furthermore, Equation (S17) becomes

$$ZT_e = \frac{< E - E_F >^2}{\sigma^2}, \qquad (S23)$$

which is clearly positive.

The mean $< E - E_F >$ and standard deviation σ capture essential features regarding the shape of *ρ(E)* and *P(E)*. Equations (S22) and (S23) reveal that *S* and ZT_e depend only on these shape parameters and are independent of L_0. Only the electrical and electronic thermal conductances depend on L_0. This feature which can be traced to the fact that $G = \frac{2e^2}{h} L_0$ and $k_e = \frac{2L_0\sigma^2}{hT}$ describe the magnitudes of currents and therefore depend on the normalization L_0 of *P(ε)*, whereas S and ZT_e involve only ratios. Clearly $< E - E_F >$ will be non-zero only if $P(E) = -T(E)\frac{\partial f(E)}{\partial E}$ is an asymmetric function of $(E - E_F)$ and since $-\frac{\partial f(E)}{\partial E}$ is a symmetric function of $(E - E_F)$, $T(E)$ should be asymmetric with respect to E_F. Examples of two candidate transmission functions are shown in Figure S7.

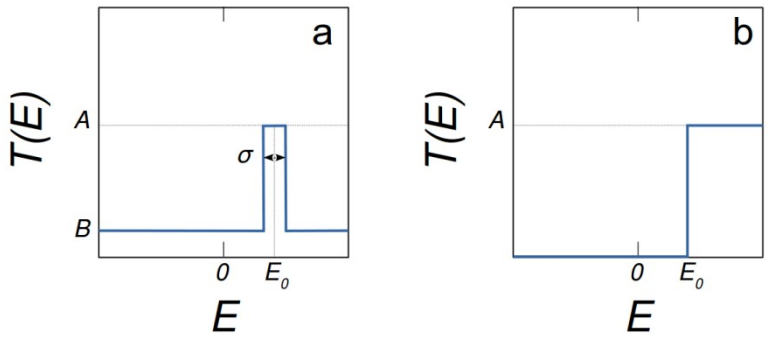

Figure S7. Two ideal transmission coefficients *T*. (a) Delta-function like *T(E)* and (b) Step-function like *T(E)*.

Figure S3a is relevant for structures, whose electronic density of states contains narrow resonances, such as single-molecule electrical junctions. Equation (S11) reveals that $ZT_e = \infty$, when $\sigma = 0$, which occurs when $T(E)$ is proportional to a delta function [64] of the form $T(E) = A\delta(E - E_0)$, in which case, $\rho(E) = \delta(E - E_0)$, $S = \frac{-1}{|e|T}(E_0 - E_F)$ and ZT_e is infinite. Similarly $G = \frac{2e^2}{h} A(-\frac{\partial f(E_0)}{\partial E_0})$ and $k_e = 0$. Thermal properties of a system with a delta-function-like transmission are shown in Figure S8.

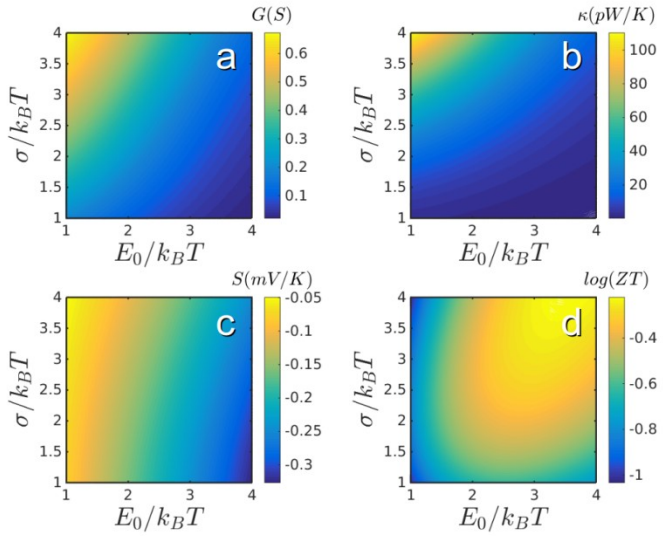

Figure S8. Thermal properties of the delta-function like *T(E),* obtained with $E_F = 0$. (a) conductance, (b) electronic thermal conductance, (c) thermopower and (d) total *ZT* by assuming a constant phonon thermal conductance. γ and σ are chosen to be 10.

<u>Strategy 3: Utilising steps in *T(E).*</u>

As alternative to using narrow transmission resonances, we now consider the step-like transmission shown in Figure S9, which occurs in periodic structures such as a crystalline lead, where *T(E)* is equal to the number of open channels and therefore changes in integer steps [65]. As a simple example, we now examine the thermopower and ZT_e of a system with a model step-like transmission coefficient of the form: $T(E) = A$ for $E>E_0$ and $T(E)=0$ for $E<E_0$, where *A* is an arbitrary constant defining the height of the step and E_0 defines the position of the step. In this case, it is convenient to introduce the dimensionless parameter $y = (E - E_F)/k_BT$, so the Fermi function takes the form $f(E)=(\exp y + 1)^{-1}$ and write Equation (S11) in the form

$$L_n = A(k_BT)^n I_n(y_0) \qquad (S24)$$

where $y_0 = (E_0 - E_F)/k_BT$,

$$I_n(y_0) = \int_{y_0}^{\infty} dy \left[-\frac{df}{dy}\right] y^n \qquad (S25)$$

and $\left[-\frac{df}{dy}\right] = e^y/(e^y+1)^2$. Clearly all moments depend only on the size of the step (ie the dimensionless parameter A) and the dimensionless parameter y_0, which defines the location of the step relative to the Fermi energy of the electrodes, in units of k_BT. In terms of I_n, $< E - E_F > = k_BT\frac{I_1}{I_0}$, $\sigma^2 = (k_BT)^2[\frac{I_2}{I_0} - \frac{I_1^2}{I_0^2}]$. Plots of the dimensionless Fermi integrals $I_n(y_0)$ are shown below.

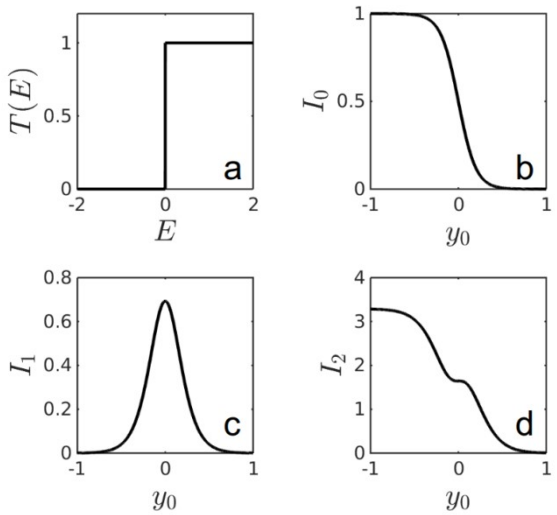

Figure S9. I_0, I_1 and I_2 for a step-function like transmission coefficient.

$$I_0(y_0) = \int_{y_0}^{\infty} dy \left[-\frac{df}{dy}\right] = f(y_0) - f(\infty) = f(y_0)$$

Clearly $I_0(\infty)$=0 and $I_0(-\infty)$=1, because . Also since $\left[-\frac{df}{dy}\right]y$ is odd, $I_1(\mp\infty)$=0 and $I_1(y_0)$ is a maximum at $y_0 = 0$. Furthermore, $I_2(-\infty) = \frac{\pi^2}{3}$ and since $\left[-\frac{df}{dy}\right]y^2 = 0 \; at \; y = 0$, the slope of $I_2(y_0)$ vanishes at $y_0 = 0$. As shown in Figure S0.

In terms of $I_n(y_0)$ the thermoelectric parameters become

$$G = \frac{2e^2}{h}AI_0, \qquad (S26)$$

$$S = \frac{k_B I_1}{e\, I_0}, \tag{S27}$$

$$k_e = \frac{2A(k_B)^2 T}{h}(I_2 - \frac{I_1^2}{I_0}), \tag{S28}$$

$$ZT_e = \left[\frac{I_1^2}{I_0^2}\right] / \left[\frac{I_2}{I_0} - \frac{I_1^2}{I_0^2}\right] \tag{S29}.$$

These equations show that the natural unit of G is $\frac{2e^2}{h} = 77\mu S$, of S is $\frac{k_B}{e} = 86\ \mu V/K$ and of k_e is $\frac{2(k_B)^2 T}{h} = 173\ pW/K$ at room temperature (ie 300K). Clearly G and k_e are both proportional to step size A, whereas S and ZT_e are independent of A. Plots of the dimensionless thermopower $\overline{S} = \frac{I_1}{I_0}$ and dimensionless electronic thermal conductance $\overline{k_e} = (I_2 - \frac{I_1^2}{I_0})$ are shown in Figure S10.

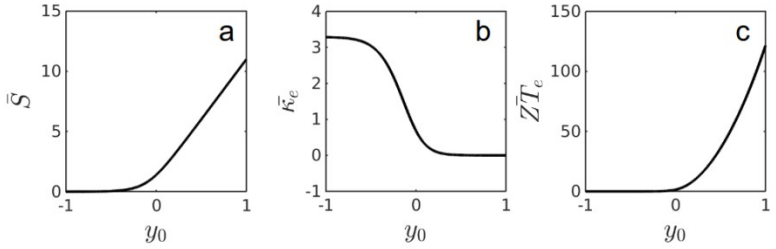

Figure S10. Dimensionless thermopower $\overline{S}(y_0) = \frac{I_1}{I_0}$ and dimensionless electronic thermal conductance $\overline{k_e} = (I_2 - \frac{I_1^2}{I_0})$ and the electronic thermoelectric figure of merit ZT_e.

Obviously, since the moments L_n in Equation (S11) are linear in *T(E)*, the above analysis can be applied to various combinations of steps. For example for the step-like transmission coefficient of the form: *T(E) = B* for *E<E₀* and *T(E)=0* for *E>E₀*, the relevant integrals are $J_n(y_0) = \int_{-\infty}^{y_0} dy \left[-\frac{df}{dy}\right] y^n$ and Equation (S24) is replaced by $L_n = B(k_B T)^n J_n(y_0)$.

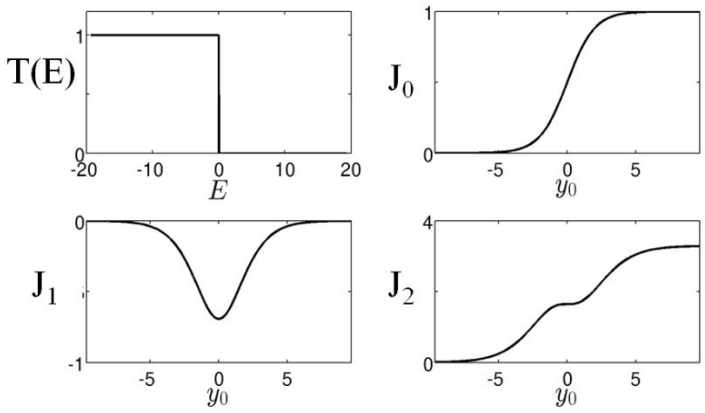

Figure S11. J_0, J_1 and J_2 for a step-function like transmission coefficient. (These can be obtained from Figure S9 by symmetry).

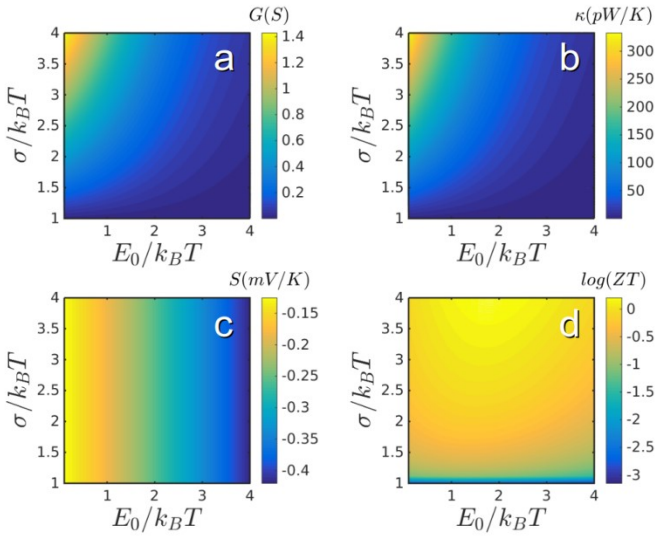

Figure S12. Thermal properties of the step-function like *T(E)*. (a) conductance, (b) electronic thermal conductance, (c) thermopower and (d) total ZT by assuming a constant phonon thermal conductance $300pW/K$. γ and σ are chosen to be 10.

Figure S12 shows an example of a graphene nanoribbon with step-function-like electron transmission coefficient around the Fermi energy $E_F = 0$ [65]. The structure is formed by two overlapping monolayer ribbons with hydrogen edge terminations, with the overlapping bilayer region containing a nanopore, whose edges are terminated by oxygen. Electrons flow from a left electrode connected to the top ribbon, to an electrode connected to the bottom ribbon, through the overlap region. Over

the energy interval shown, there is one open scattering channel in the crystalline nanoribbons. In this case the oxygen-terminated pore blocks electron transmission over the energy interval 0 to 0.2 eV and an asymmetric step in *T(E)* arises from the asymmetry created by the presence of the oxygens.

We discussed some principles underpinning strategies for enhancing their thermoelectric performance. The latter include (a) taking advantage of steep slopes in *T(E),* (b) creating structures with delta-function-like transmission coefficients and (c) utilising step-like features in *T(E)*. To achieve high performance, these strategies should be combined with methods for reducing inhomogeneous broadening and minimising the phonon thermal conductance.

A comparison between DFT-GGA and DFT-GAA+U for the metallo-porphyrin nanotube PFe.

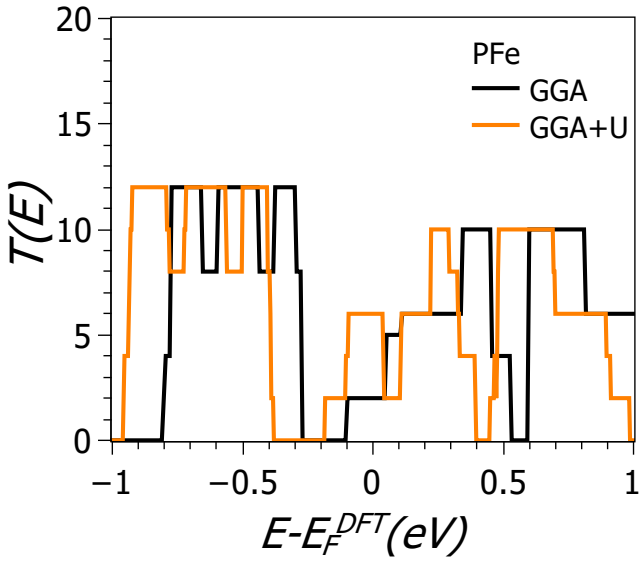

Figure S13. shows the comparison between DFT-GGA and DFT-GAA+U calculations of transmission coefficient $T(E)$ versus energy for the metallo-porphyrin nanotube PFe.

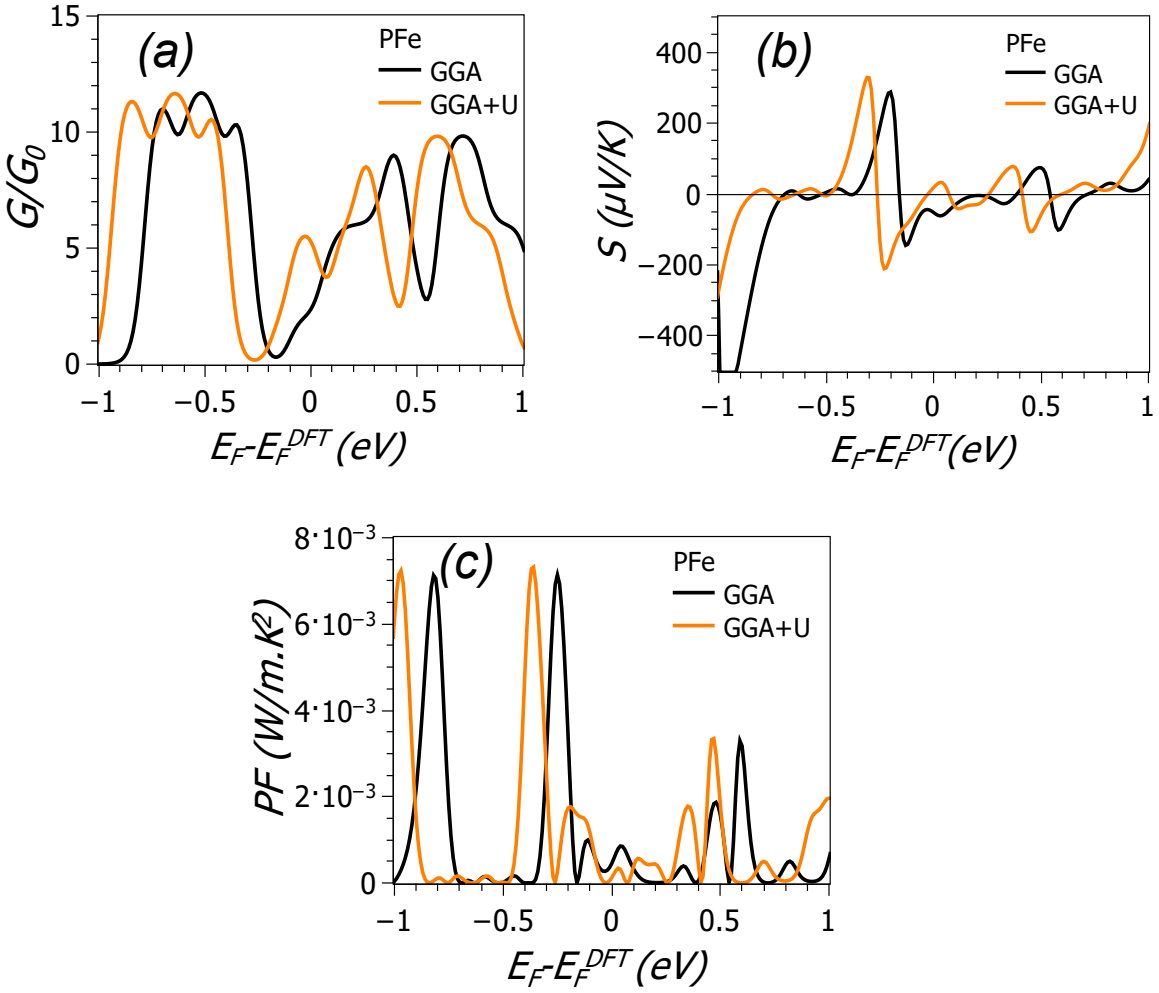

Figure S14. shows the comparison between DFT-GGA and DFT-GAA+U calculations for thermoelectric coefficients, where *(a)* room-temperature electrical conductance, *(b)* the thermopower *S* and *(c)* power factor $PF = \sigma S^2$ over a range of Fermi energies for the metallo-porphyrin nanotube PFe.

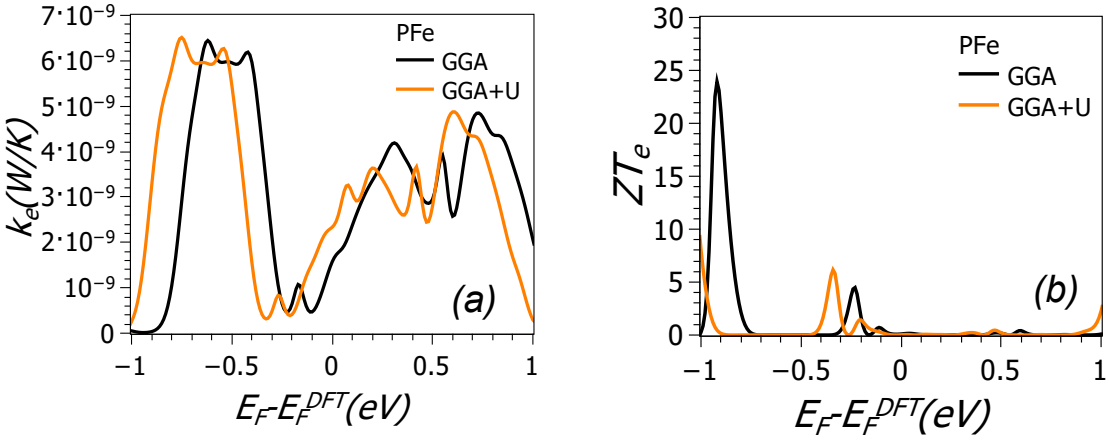

Figure S15. shows the corresponding results for electronic contribution to the *(a)* thermal conductance k_e and *(b)* figure of merit ZT_e versus Fermi energy.

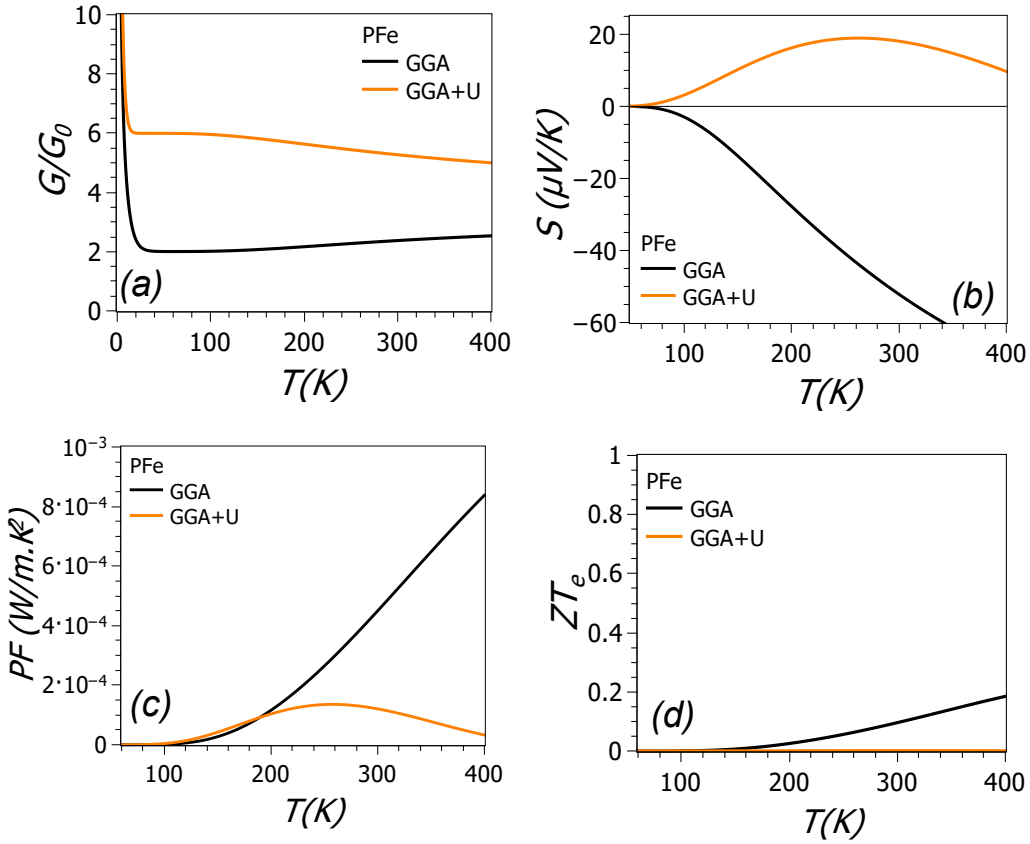

Figure S16. shows the comparison between DFT-GGA and DFT-GAA+U calculations for thermoelectric coefficients versus temperature T, where *(a)* the electrical conductance, *(b)* thermopower S, *(c)* power factor $PF = \sigma S^2$ and *(d)* electronic figure of merit ZT_e evaluated at $E_F - E_F^{DFT} = 0\ eV$ for the metallo-porphyrin nanotube PFe.

A comparison between DFT-GGA and DFT-GAA+U for the metallo-porphyrin nanotube PFe-Cl

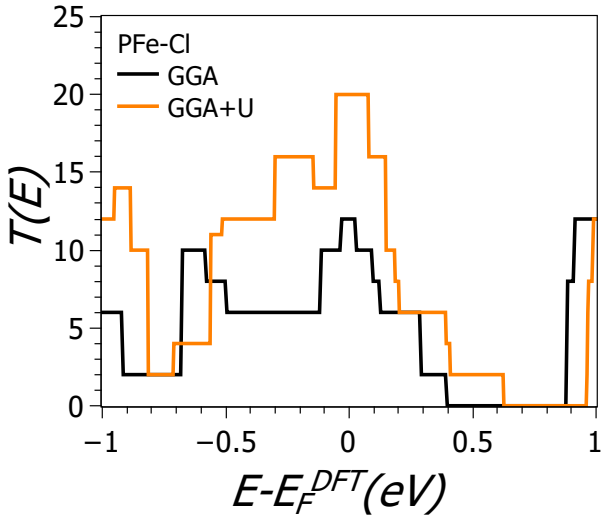

Figure S17. shows the comparison between DFT-GGA and DFT-GAA+U calculations of transmission coefficient $T(E)$ versus energy for the metallo-porphyrin nanotube PFe in presence of a Cl^- counter ion.

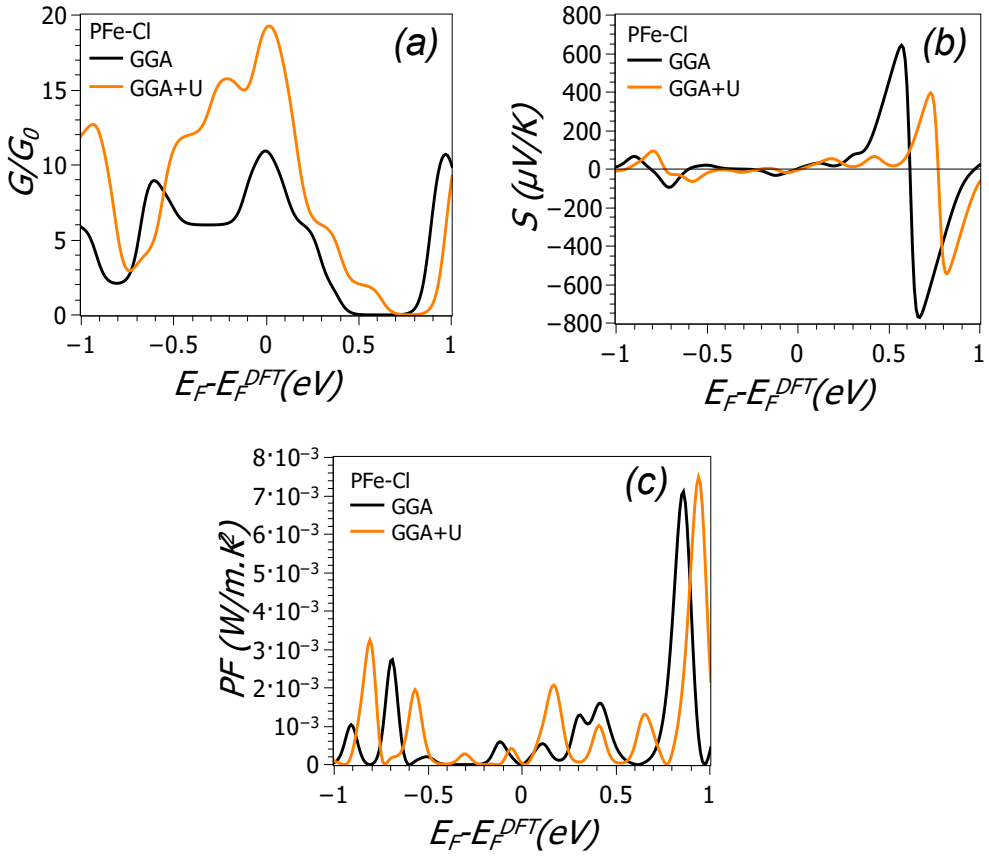

Figure S18. shows the comparison between DFT-GGA and DFT-GAA+U calculations for thermoelectric coefficients, where *(a)* room-temperature electrical conductance, *(b)* the thermopower *S* and *(c)* power factor $PF = \sigma S^2$ over a range of Fermi energies for the metallo-porphyrin nanotube PFe in presence of a Cl^- counter ion.

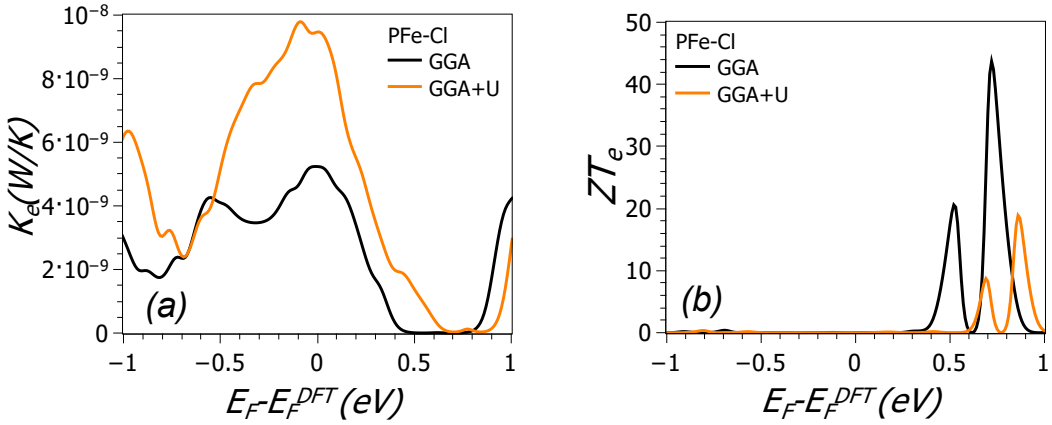

Figure S19. shows the corresponding results for electronic contribution to the *(a)* thermal conductance k_e and *(b)* electronic figure of merit ZT_e versus Fermi energy.

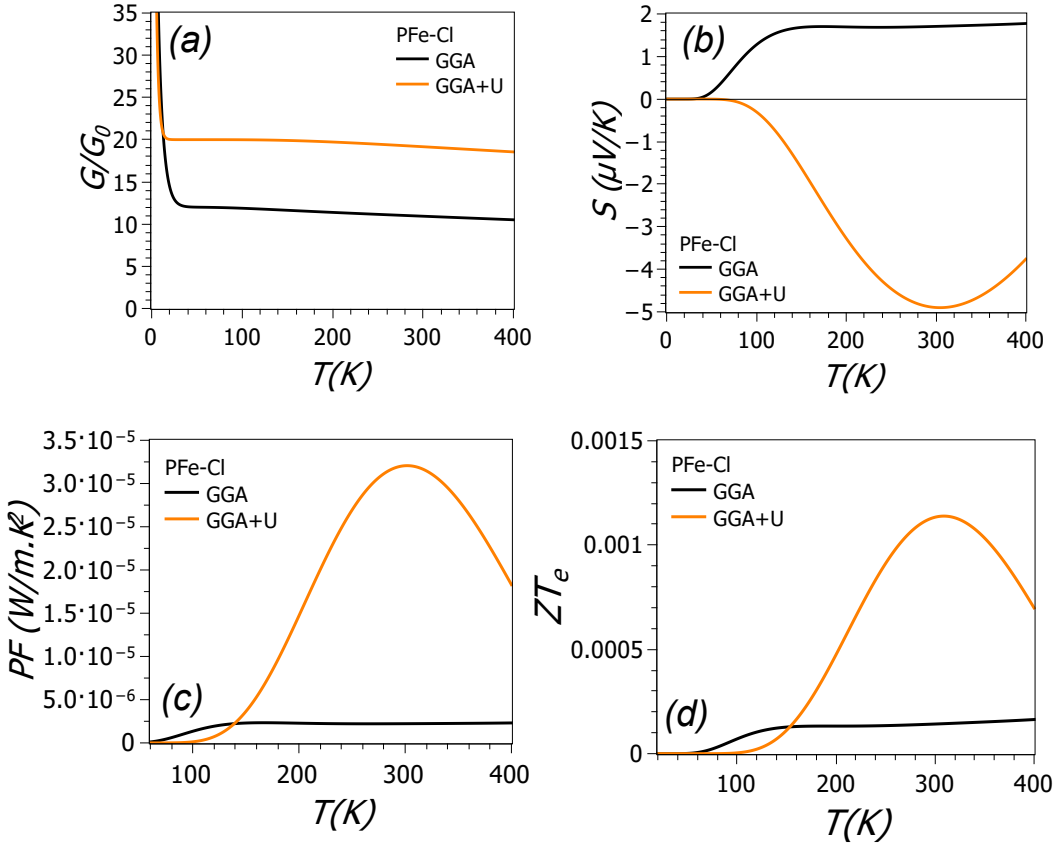

Figure S20. shows the comparison between DFT-GGA and DFT-GAA+U calculations for thermoelectric coefficients versus temperature *T*, where *(a)* the electrical conductance, *(b)* thermopower *S*, *(c)* power factor $PF = \sigma S^2$ and *(d)* electronic figure of merit ZT_e evaluated at $E_F - E_F^{DFT} = 0\ eV$ for the metallo-porphyrin nanotube PFe in presence of a Cl^- counter ion.

References

1. Finch, C., V. Garcia-Suarez, and C. Lambert, *Giant thermopower and figure of merit in single-molecule devices.* Physical Review B—Condensed Matter and Materials Physics, 2009. **79**(3): p. 033405.
2. García-Suárez, V.M., et al., *Redox control of thermopower and figure of merit in phase-coherent molecular wires.* Nanotechnology, 2014. **25**(20): p. 205402.
3. Algharagholy, L.A., et al., *Tuning thermoelectric properties of graphene/boron nitride heterostructures.* Nanotechnology, 2015. **26**(47): p. 475401.